



This is a repository copy of *A novel time-varying modelling and signal processing approach for epileptic seizure detection and classification*.

White Rose Research Online URL for this paper:
<https://eprints.whiterose.ac.uk/165418/>

Version: Accepted Version

Article:

Wang, Q., Wei, H. orcid.org/0000-0002-4704-7346, Wang, L. et al. (1 more author) (2021) A novel time-varying modelling and signal processing approach for epileptic seizure detection and classification. *Neural Computing and Applications*, 33 (11). pp. 5525-5541. ISSN 0941-0643

<https://doi.org/10.1007/s00521-020-05330-7>

This is a post-peer-review, pre-copyedit version of an article published in *Neural Computing and Applications*. The final authenticated version is available online at: <http://dx.doi.org/10.1007/s00521-020-05330-7>.

Reuse

Items deposited in White Rose Research Online are protected by copyright, with all rights reserved unless indicated otherwise. They may be downloaded and/or printed for private study, or other acts as permitted by national copyright laws. The publisher or other rights holders may allow further reproduction and re-use of the full text version. This is indicated by the licence information on the White Rose Research Online record for the item.

Takedown

If you consider content in White Rose Research Online to be in breach of UK law, please notify us by emailing eprints@whiterose.ac.uk including the URL of the record and the reason for the withdrawal request.



eprints@whiterose.ac.uk
<https://eprints.whiterose.ac.uk/>

A Novel Time-Varying Modelling and Signal Processing Approach for Epileptic Seizure Detection and Classification

Qinghua Wang^{1,†} · Hua-Liang Wei^{2,†} · Lina Wang¹ · Song Xu¹

Received:

© The Natural Computing Applications Forum 2020

Abstract

Electroencephalogram (EEG) signal analysis plays an essential role in detecting and understanding epileptic seizures. It is known that seizure processes are nonlinear and nonstationary, discriminating between rhythmic discharges and dynamic change is a challenging task in EEG based seizure detection. In this paper, a new time-varying (TV) modeling framework, based on an autoregressive (AR) model structure, is proposed to characterize and analyze EEG signals. The TV parameters of the AR model are approximated through a multi-wavelet basis function expansion (MWBF) approach. An effective ultra-regularized orthogonal forward regression (UROFR) algorithm is employed to significantly reduce and refine the resulting expanded model. Given a time-varying process, the proposed TVAR-MWBF-UROFR method can generate a parsimonious TVAR model, based on which a high-resolution power spectrum density (PSD) estimation can be obtained. Informative features are then defined and extracted from the PSD estimation. The TVAR-MWBF-UROFR method is applied to a number of real EEG datasets; features obtained from these datasets are then used for seizure detection and classification. To make the results more accurate and reliable, a PCA algorithm is adopted to select the optimal feature subset, and a Bayesian optimization technique based on the Gaussian process (GP) is performed to determine the coefficients associated with each of the classifiers. Experimental results of the proposed approach outperform the compared state-of-the-art classifiers on two benchmark datasets. Moreover, the results produced by the proposed time-frequency analysis scheme are more reliable for seizure detection based on the noisy EEG datasets used in our case studies.

Keywords: electroencephalogram (EEG) · epileptic seizure detection · time-varying process · ultra-regularized orthogonal forward regression (UROFR) · time-frequency analysis · Bayesian optimization

1 Introduction

Epilepsy is a widespread and high-risk chronic disease [1]. The pathological cause of epilepsy in individuals is generally unexplained and the mechanisms behind seizure remain unknown [2]. The prevalence of epilepsy worldwide can be as high as 5% of the general population, and appro-

ximately 80% of the people who have epilepsy are in developing countries [3]. EEG signal contains various useful information relating to numerous physiological states of the brain and thus is an indispensable tool for understanding brain diseases, such as epilepsy [4]. Classically, clinical diagnosis of epileptic seizures relied primarily on clinical examination and visual observations of EEG records, which was often time-consuming and subjective [5,6]. Therefore, it is of considerable significance to develop an effective automatic epileptic EEG signal classification system to improve the efficiency and reliability of timely epilepsy diagnosis. The crucial factor in EEG recognition is to extract valuable features to describe EEG signal characteristics and exploit them for classification purposes [7,8].

Studies over the past two decades have provided valuable information on epilepsy detection [9]. In [10], feature extraction methods based on the waveform feature of EEG signals were briefly reviewed. However, due to the apparent rhythmicity and non-stationarity of EEG signals, feature extraction based on waveforms can only obtain partial

✉ Lina Wang
sy1803113@buaa.edu.cn
Qinghua Wang
zchan@buaa.edu.cn
Hua-Liang Wei
w.hualiang@sheffield.ac.uk

¹ National Laboratory of Aerospace Intelligent Control Technology, Beijing Aerospace Automatic Control Institute, China

² Department of Automatic Control and Systems Engineering, University of Sheffield, United Kingdom

† These authors contributed equally to this work.

information [11,12]. Some scholars have tried to extract

proposed to refine and reduce the TVAR model structure

features of EEG signals using more complex time-frequency analysis methods. For example, Gandhi et al. [13] characterized the energy, variance and information entropy of EEG signals in a frequency band and studied the characteristics of EEG signals using wavelet functions. Guo et al. [14] employed a multi-scale wavelet transform to decompose EEG signals and took approximate entropy of each frequency band as the characteristics of EEG signals. In 2013, Li et al. [15] extracted the variance, fluctuation index and other components from the Intrinsic Mode Functions (IMF) after EMD decomposition as epileptic EEG features. Faust et al. [16] utilized a DWT-based technique for EEG denoising and feature extraction in epilepsy diagnosis, and their results demonstrated that the wavelet method was a practical method for automatic seizure detection using EEG signals. In addition, Wani et al. [17] used the energy distribution of wavelet coefficients in each sub-band frequencies of the EEG records and adopted an Artificial neural network (ANN) for classification. Their seizure detection approach can efficiently recognize epileptic seizures and thus alleviate the burden of medical professionals. Non-parametric time-frequency analysis methods such as STFT and CWT have also been widely adopted in EEG signal analysis, but most of these methods are sensitive to noise and normally suffer from the issue of a trade-off between temporal and frequency resolutions [18,19]. Those shortages usually reduce the performance of the extracted features from EEG signals [20,21].

Unlike those aforementioned nonparametric spectral approaches, the power spectral density (PSD) estimation based on the time-varying autoregressive (TVAR) model is a parametric time-frequency analysis method, which overcomes the deficiency of time-frequency resolution given by STFT and CWT methods [21]. Due to its straightforward structure and the allowance of time-varying parameters, the TVAR model, as a simplified nonlinear model, provides an effective tool to reveal the dynamic characteristics of non-stationary time series such as EEG signal [22-24]. However, the ongoing challenge is to construct a sufficiently accurate TVAR model [21-23].

The central objective of this study is to develop an effective tool for epileptic seizure detection and classification based on EEG recordings. In doing so, we propose a novel efficient TVAR-MWBF-UROFR approach, which can yield a parsimonious TVAR model with satisfying generalization ability to process, characterize and analyze EEG signals. Fig. 1 presents the schematic diagram of the proposed scheme for epileptic seizure detection. First of all, a new multi-resolution wavelet expansion method is introduced to approximate each of the time-varying parameters of the TVAR model. Then a novel ultra-regularized orthogonal forward regression algorithm (called UROFR), incorporating derivative information, is

and estimate the corresponding parameters. Secondly, a PSD function is defined based on the reduced TVAR model, and the time-frequency features then extracted in five frequency sub-bands according to clinical experience. Finally, a PCA approach is exploited to reduce the dimensionality of the extracted feature spaces, and the best-identified classifier is obtained via a Bayesian optimization technique. Our proposed scheme is applied to several publicly available EEG datasets and experimental results demonstrate that the proposed approach outperforms most existing methods in terms of sensitivity (SEN), specificity (SPE), and accuracy (ACC). Additionally, we also preliminarily explored the robustness of the proposed method for classification of seizure EEG from non-resting EEG with muscle artifacts, and the accuracy has remained above 95% for epilepsy detection. These results suggest that the proposed TVAR-MWBF-UROFR approach is robust for seizure detection and classification.

The remainder of the paper is arranged as follows. The second section introduces the EEG data used for the experiments and section 3 is concerned with the methodology used for this study. Section 3.1 details the proposed TVAR-MWBF-UROFR algorithm. Model order determination is presented in Section 3.2. High-resolution time-frequency analysis based on power spectral density is depicted in Section 3.3. Section 3.4 illustrates the classification and performance evaluation. Results of the experiment are presented in Section 4. Detailed discussions about the effectiveness of the proposed method and its limitations are given in Section 5. Finally, Section 6 summarizes our main work and offers possible future extensions.

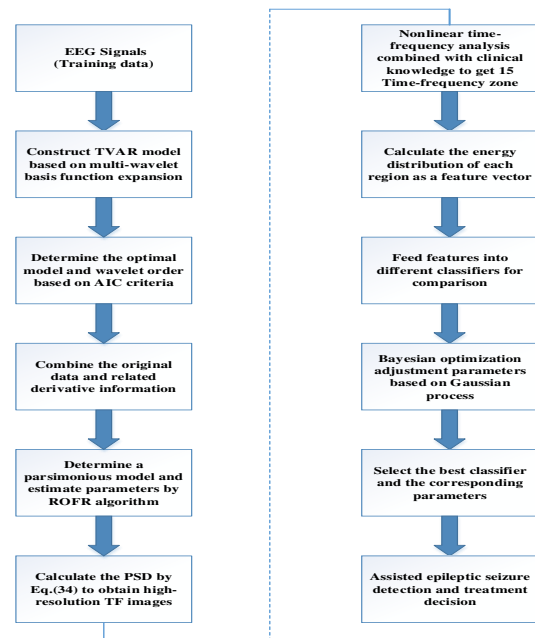


Fig. 1 The schematic diagram of the proposed method for epileptic seizure detection.

2 Dataset Description

We perform comparative experiments on two independent EEG datasets to verify the general applicability of our proposed method. Dataset 1 was acquired from Bonn University, and Dataset 2 was collected from Neurology and Sleep Centre(NSC), New Delhi.

2.1 Description of Dataset 1

The EEG dataset includes five subsets, denoted as Z, O, F, N, and S, respectively [25]. Each subset consists of 100 single-channel EEG records of a duration of 23.6 s, at a sampling rate of 173.61Hz. Subset Z and O involve surface EEG signals recorded from five healthy participants with the EEG electrode arranged using an international 10–20 system. Subjects were awake and relaxed with eyes-open (Set Z) and eyes-closed (Set O) in the recording process. The other three subsets N, F, and S contain intracranial EEG signals taken from five epileptic patients undergoing preoperative assessment. Subsets N and F were recorded in seizure-free intervals from five epileptic patients in the epileptogenic zone (set F) and the hippocampal formation of the opposite hemisphere of the brain (set N). EEG segments in subset S consists of data recordings during a seizure (ictal) event. All EEG records were recorded by the same 128-channel amplifier system with the equal average reference value, undergoing preliminary processing to remove artifacts, interference, etc[5,18]. This paper carries out four types of EEG signal classification tasks: S/Z, S/N, S/F, S/NF. These four EEG signal classification tasks are of great significance in clinical practice and have been widely adopted by researchers.

2.2 Description of Dataset 2

The second dataset contains segmented EEG records of ten epilepsy patients, and it is freely available at <https://www.researchgate.net/publication/308719109>. All EEG recordings were attained at a sampling rate of 200 Hz utilizing the GrassTelefactor Comet AS40 amplification system, and the EEG record length of each trial is about 5.2 s (1024 samples). During the recording period, gold plated scalp EEG electrodes were placed on the surface of the brain according to the 10-20 standard. The signals were first filtered using a band-pass filter with cut-off frequencies of 0.5 Hz and 70 Hz and then classified into pre-ictal (Set A), inter-ictal (Set B), and ictal (Set C) stages by clinical experts. To verify the performance of the proposed approach in recognizing scalp seizure EEG signals, we performed four classification tasks C/A, C /B, C/AB, and A/B.

3 Methodology

3.1 Identification of time-varying models based on the new TVAR-MWBF-UROFR approach

In this section, a new TVAR-MWBF-UROFR approach that provides useful information in the time-frequency domain is introduced. Specifically, the MWBF expansions are first utilized to approximate TV coefficients in the TVAR model, and the UROFR algorithm is then applied to refine and reduce the full NWBF expansion model to result in a parsimonious model with satisfactory generalization ability.

3.1.1 Basis function expansions of the time-varying AR models

A time-varying AR model of order p is formulated as [21-23,26]:

$$y(t) = \sum_{i=1}^p a_i(t)y(t-i) + e(t) \quad (1)$$

where $y(t)$ is the time-varying signal to be modeled, t is a discrete-time sampling instant; p is the model order, $a_i(t)$, with $i=1,2,\dots, p$, represents the i -th model parameter, and $e(t)$ is a stationary white noise sequence with zero mean and variance σ_e^2 .

Generally, the time-varying parameters $a_i(t)$ can be expanded to a set of basis functions $\varphi_m(t)$ for $m=1,2,\dots,M$, where M is the total number of the basis functions involved. The time-varying model in (1) can then be written as:

$$a_i(t) = \sum_{m=1}^M c_{i,m} \varphi_m(t), i = 1, 2, \dots, p \quad (2)$$

where $c_{i,m}$ are time-invariant weighting coefficients of the basis function $\varphi_m(t)$.

Substituting (2) into (1), yields:

$$y(t) = \sum_{i=1}^p \sum_{m=1}^M c_{i,m} \varphi_m(t) y(t-i) + e(t) \quad (3)$$

We now define the following new variables:

$$y_m(t-i) = \varphi_m(t) y(t-i) \quad (4)$$

Substituting (4) into (3), yields:

$$y(t) = \sum_{i=1}^p \sum_{m=1}^M c_{i,m} y_m(t-i) + e(t) \quad (5)$$

Equation (5) represents that the TVAR model has now been converted to a standard time-invariant linear AR model, where the time-invariant coefficients are $c_{i,m}$, with $i=1,2,\dots,p$; $m=1,2,\dots,M$.

Denote:

$$\Phi(t) = [\varphi_1(t), \varphi_2(t), \dots, \varphi_M(t)]^T$$

$$\Psi_M = [\psi_1, \psi_2, \dots, \psi_N]^T$$

$$\Psi(t) = [y(t-1)\varphi(t)^T, y(t-2)\varphi(t)^T, \dots, y(t-p)\varphi(t)^T]^T$$

where the superscript T denotes the transpose of a matrix or vector. Equation (3) can be written in matrix form:

$$y = \Psi_M c + e \quad (6)$$

where Ψ_M is a $N \times M$ regression matrix, $c = [c_{1,1}, c_{1,2}, \dots, c_{1,M}, \dots, c_{p,M}]^T$ is the time-invariant expansion

coefficient vector. The identification problem of the TVAR model can now be simplified to a time-invariant regression problem that can be solved using a least-squares type of algorithms.

3.1.2 Analysis of the multi-wavelet basis functions

Under certain assumptions and considerations, multi-resolution analysis (MRA) can be utilized to construct orthogonal wavelet systems. Referring to wavelet theory [27,28], a square-integrable scalar function $f(t) \in L^2(R)$ can be arbitrarily approximated using multiresolution wavelets decomposition:

$$f(x) = \sum_k a_{j_0,k} \phi_{j_0,k}(x) + \sum_{j \geq j_0} \sum_k d_{j,k} \Psi_{j,k}(x) \quad (7)$$

That is to say, the function $f(x)$ can be expressed by a linear combination of functions $\phi_{j,k}$ and $\Psi_{j,k}(x)$, where the mother wavelet family $\Psi_{j,k}(x) = 2^{j/2} \psi(2^j x - k)$ and the father wavelet family $\phi_{j,k} = 2^{j/2} \phi(2^j x - k)$ are orthonormal basis; $j, k \in Z$ (i.e., the set of all integers) are the scale and translation parameters, $a_{j_0,k}$ and $d_{j,k}$ are the wavelet decomposition coefficients, and j_0 is an arbitrary integer representing the coarsest resolution or scaling level.

In real applications, in order to exploit the functional properties of different types of wavelets to sufficiently capture the inherent dynamics of the original data, the time-varying parameters $a_i(t)$ in TVAR model (1) can be expanded with truncated wavelet expansion as [22,23]:

$$a_i(t) = d_{-1,0}^{(i)} \phi(t) + \sum_{j \geq 0} \sum_{k \geq 0} d_{j,k}^{(i)} \Psi_{j,k}(t) \quad (8)$$

where $d_{j,k}^{(i)}$ are the wavelet coefficients for the i -th time-varying parameters $a_i(t)$. $\phi(t)$ is called the scale function and $\Psi_{j,k}(t)$ is the mother basis functions. Once the scaling function and the mother wavelet are determined, the task of estimating the TV coefficients is to determine the coefficients $d_{j,k}^{(i)}$ of each wavelet. More explanations for (8) will be given in the following paragraphs. Note that multiple wavelet basis function decomposition is different from multiresolution decomposition, the former utilizes different types of wavelets to approximate a given signal, whereas the latter adopts a set of orthogonal wavelet basis functions to obtain a multiresolution approximation to a signal. Interested readers are referred to [21-23] or more details.

Although many functions can be selected as scaling or wavelet functions, most of them are not applicable to dynamic system identification, especially in the case of multi-dimensional and multi-resolution expansions. An implementation, which has been proved to be valid for dy-

namic process modeling, is to use cardinal B-splines [29,30]. Given a set of knots $s_0, s_1, \dots, s_N, N \geq n+1$. A set

of n -th order B-spline basis function can be calculated by the following recursive formula:

$$B_{i,n}(x) = \frac{x-s_i}{s_{i+n}-s_i} B_{i,n-1}(x) + \frac{s_{i+1}-x}{s_{i+1}-s_{i+2}} B_{i+1,n-1}(x) \quad (9)$$

The index i denotes the location of the B-spline basis function, and the second index n indicates the order of the B-spline functions. $(N-n)$ -th order B-spline basis function can then be determined by N knots. When the knots are even distribution, the function $B_{i,n}(x)$ is a time shift of $B_{0,n}(x)$. The first order cardinal B-spline is the very famous Harr wavelet defined as [28]:

$$B_{0,1}(x) = \begin{cases} 1, & x \in [s_0, s_1] \\ 0, & \text{other} \end{cases} \quad (10)$$

In most cases, the initial value of the position i can be chosen to be zero. In practical applications, the second-order, third-order, fourth-order, and fifth-order cardinal B-splines $B_2(x)$, $B_3(x)$, $B_4(x)$ and $B_5(x)$ are commonly used, whose explicit formulas are given in the reference [22].

Among many commonly used basis functions, the B-spline function is unique in that it has three excellent features, namely, compact support, multi-resolution analysis, and an explicit analytical form [30]. These properties make the operation of the multiresolution decomposition even more accessible and enable B-splines applicable for non-stationary signals processing and modelling. Given that the n -th order B-spline is defined on $[0, n]$, the scale and shift indices j and k for the family of the function are $\Psi_{j,k}(x) = 2^{j/2} B_n(2^j x - k)$ should satisfy $0 \leq 2^j x - k \leq n$. Suppose that the function $f(x)$ to be estimated with decompositions is defined within $[0,1]$, Then for any scale factor j , the practical values for the shift index k are constrained to the collection $\Gamma_n = \{k: -n \leq k \leq 2^j - 1\}$.

Note that while the first- and second-order B-splines are non-smooth piecewise functions, they are very useful for signals with similar bursts and sharp transients, and higher-order B-splines can better fit smoothing signals [30]. B-splines of order 1 to 5 are preferred in many real applications. The unique nature of the B-spline basis function makes multi-resolution decomposition calculations more compact and convenient. Time-varying parameters $a_i(t)$ in the TVAR model (1) can be expanded with multi-wavelet basis functions from the families $\{\psi_k^{(n)}: n = 1, \dots, 5; k \in \Gamma_n\}$. For instance, below is an expression of a combination of the families for the i -th model parameter:

$$a_i(t) = \sum_{k \in \Gamma_s} d_{i,k}^{(s)} \psi_{j,k}^{(s)}\left(\frac{t}{N}\right) + \sum_{k \in \Gamma_q} d_{i,k}^{(q)} \psi_{j,k}^{(q)}\left(\frac{t}{N}\right) + \sum_{k \in \Gamma_l} d_{i,k}^{(l)} \psi_{j,k}^{(l)}\left(\frac{t}{N}\right) + \sum_{k \in \Gamma_r} d_{i,k}^{(r)} \psi_{j,k}^{(r)}\left(\frac{t}{N}\right) \quad (11)$$

where $1 \leq q \leq s \leq l \leq r \leq 5$, $t=1,2,\dots,N$ and N is the length of the observation sequence. Experience from previ-

ous studies shows that for most time-varying problems, the choice of $r=1$, $l=2$, $q=3$, $s=4$ and $j=3$ perform well to regain

the time-varying parameters. The decomposition (11) can easily be converted to formula (2), where the collection $\varphi_m(t)$ for $m=1,2,\dots,M$ is replaced by the union of the four families: $\Psi_{j,k}^{(n)}(t)$, $k \in \Gamma_n$, n from 1 to 4. Further derivation can then lead to the standard linear regression equation:

$$y(t) = \sum_{i=1}^p \sum_{j>j_0} \sum_n \sum_{k \in \Gamma_n} d_{i,k}^{(n)} \Psi_{j,k}^{(n)}\left(\frac{t}{N}\right) y(t-i) e(t) \quad (12)$$

where $\sum_{i=1}^p \sum_n \sum_{k \in \Gamma_n} d_{i,k}^{(n)} = \sum_{i=1}^p \sum_{m=1}^M c_{i,m}$.

3.1.3 Ultra-Least Square Method for TVAR Model

The objective of model structure detection is to select essentially important model regressors and build a parsimonious model. In practice, not all the terms in the MWBF-based model are significant; some may be redundant and can be removed from the model [31]. Consequently, it is necessary to detect important model terms that should be involved in the MWBF-based expansion model. For identifying dynamic systems, where individual observed data points are time-correlated and may be interconnected in the derivative space of time-continuous functions, which can reveal many relevant features of the system. However, the standard least-squares regression can only utilize partial information hidden in the observation data, ignoring the connection between the observed data points, and thus cannot find the difference in each time instance. All this can lead to overfitting of the least-squares regression model. [32,33].

In this study, a surrogate criterion called ultra-least-squares (ULS) is introduced to improve the model representation and generalization ability. In addition, the regularized orthogonal forward regression (ROFR) algorithm, incorporating the zero-th order regular term with the orthogonal forward regression (OFR) algorithm, is used to enhance the robustness of the parameter estimation and prevent the overfitting issue while the calculation amount is equivalent to the OFR algorithm. Compact pseudo-code with some specific details of the ROFR algorithm is given in the Appendix. The ULS criterion is combined with the convenient ROFR algorithm to produce a novel ultra-regularized orthogonal forward regression (called UROFR) algorithm for nonlinear system identification. In many modeling tasks, the UROFR algorithm has proven to be robust for model structure detection and is more promising to provide an optimal model. The generic parametric linear problem (12) can be solved utilizing a least-

squares type of algorithm by minimizing the corresponding loss function:

$$J_{LS} = \left\| y - \sum_{i=1}^p \sum_n \sum_{k \in \Gamma_n} d_{i,k}^{(n)} x_{i,k}^{(n)} \right\|_2^2 \quad (13)$$

where $x_{i,k}^{(n)} = \sum_{j>j_0} \Psi_{j,k}^{(n)}\left(\frac{t}{N}\right) \cdot y(t-i)$ is an expanded term, and $d_{i,k}^{(n)}$ is the corresponding time-invariant parameter. Unlike the ordinary least-squares criterion concerning model fitting in the L_2 space, the ULS criterion considers model fitting in a sub-space, called Sobolev space, which is a collection of functions defined on $[0, T]$. Mathematically, this space is defined as

$$H^m([0, T]) = \{x(t) \in L^2([0, T]) | D^l x \in L^2([0, T]), l = 1, 2, \dots, m\} \quad (14)$$

In the Sobolev space, the ULS approach enables to reveal useful inter-correlation information between signals which otherwise cannot be revealed by most least-squares type of algorithms. ULS utilizes information about weak derivatives of signals. For any smooth test function $\varpi(t) \in C_0^\infty([0, T])$ has compact support on $[0, T]$, the weak derivatives $D^l x(t)$ of a signal $x(t)$ satisfy:

$$\int_{[0, T]} x(t) D^l \varpi(t) dt = (-1)^l \int_{[0, T]} \varpi(t) D^l x(t) dt \quad (15)$$

Note that the weak derivatives of up to m -th order are L^2 integrable on any finite interval $[0, T]$. It can be proved that if the l -th order weak derivative of a function exists, the derivative is unique in the sense that it is almost zero everywhere. This study adopted test functions to smooth the observed data, and it would be preferable for such functions to satisfy a bell-shape resemble a Gaussian function. In practice, test functions do not necessarily have infinitely differentiable, any function with functional properties, such as cubic B-spline basis function, can be adopted as the modulating function, whose first and second derivatives of the smoothed data are considered in the ULS criterion.

In this paper, a new metric, defined in the Sobolev space $H^m([0, T])$, which is useful for revealing hidden information buried in observational data is introduced. The H^m norm associated with the new metrics is defined as:

$$\|x\|_{H^m} = \sqrt{\sum_{l=0}^m \|D^l x\|_2^2} \quad (16)$$

where D^l represents the l -th order differentiation operator. Since differentiation is a linear operator, under the new proposed ULS criterion, model (12) can be written as:

$$J_H = \left\| y - \sum_{i=1}^p \sum_n \sum_{k \in \Gamma_n} d_{i,k}^{(n)} x_{i,k}^{(n)} \right\|_2^2 + \sum_{l=1}^m \|D^l y - \sum_{i=1}^p \sum_n \sum_{k \in \Gamma_n} d_{i,k}^{(n)} D^l x_{i,k}^{(n)}\|_2^2 \quad (17)$$

The lost function (17) comprises two parts: the first part is consistent with the standard least-squares norm that emphasizes the global similarity; the second part is the weak

derivatives that focus on the details and compactness of the data points. In this part, any subtle difference in the overall distribution can be reflected clearly. It is the second part that makes it more useful for dynamic system identification.

In combination with the H^m criterion, the procedure modifies to solve an improved least-squares equation:

$$\begin{bmatrix} y \\ D^1 y \\ \vdots \\ D^m y \end{bmatrix} = \sum_{i=1}^p \sum_n \sum_{k \in \Gamma_n} d_{i,k}^{(n)} \begin{bmatrix} x_{i,k}^{(n)} \\ D^1 x_{i,k}^{(n)} \\ \vdots \\ D^m x_{i,k}^{(n)} \end{bmatrix} \quad (18)$$

The introduction of the weak derivatives based on the locally defined test function $\varpi(t)$ can reveal valuable differential information in a time series. Different positions of the test function along the time axis produce various test functions, and the correlated weak derivative contains local information about the signal in a new location. Thus, instead of using overall test functions in the space $C_0^\infty([0, T])$, a locally defined test function $\varpi(t)$ and its time-shifted versions $\varpi(t - \tau)$ are used in the new ULS criterion.

For a given test function $\varpi(t)$ with finite support on $[0, T_0]$, ($T_0 < T$), the distribution $\langle D^l T_y, \varpi(t - \tau) \rangle$ can be viewed as a function of τ , which can be defined as:

$$y^l(\tau) = \langle D^l T_y, \varpi(t - \tau) \rangle = (-1) \int_0^T y(t) \varpi(t - \tau) dt, \tau \in [0, T - T_0] \quad (19)$$

where $y^l(\tau)$ indicates the convolution of $y(t)$ with the l -th derivative of the test function. Denote $g(t) = \varpi(-t)$, then the weight function $g^{(l)}(t)$ can be considered as the impulse response of a linear filter and $y^l(\tau)$ is the corresponding output driven by the input signal $y(t)$. From the Leibniz integral rule, the order of differentiation and integration allows for interchange. In particular, the differential under the integral sign satisfies:

$$\frac{d^l}{dt^l} \int_0^t y(\tau) g(t - \tau) d\tau = \int_0^t y(\tau) \frac{\partial^l}{\partial t^l} g(t - \tau) d\tau = \int_0^t y(\tau) \frac{d^l}{dt^l} g(t - \tau) d\tau \quad (20)$$

Now the newly proposed functions $y^l(\tau)$ have a clear physical explanation. The function $y^l(\tau)$ smooths the data first and later calculates the derivatives of the smoothed data. Likewise, the functions $(x_{i,k}^{(n)})^l(\tau)$ can be expressed as:

$$(x_{i,k}^{(n)})^l(\tau) = \langle D^l T_{x_{i,k}^{(n)}}, \varpi(t - \tau) \rangle = (-1) \int_0^T x_{i,k}^{(n)} \varpi^l(t - \tau) dt \quad (21)$$

Then, the ULS problem (18) becomes:

$$\begin{bmatrix} y \\ y^1 \\ \vdots \\ y^m \end{bmatrix} = \sum_{i=1}^p \sum_n \sum_{k \in \Gamma_n} d_{i,k}^{(n)} \begin{bmatrix} x_{i,k}^{(n)} \\ (x_{i,k}^{(n)})^1 \\ \vdots \\ (x_{i,k}^{(n)})^m \end{bmatrix} \quad (22)$$

where y^l and $(x_{i,k}^{(n)})^l$ are the associated derived functions defined by (19) and (21). There is a potential issue with the J_H criterion given by (17) when applied to system identification in that the difference arising from the derivatives constitute a bigger proportion than that arising from the data themselves, that is:

$$\sum_{l=1}^m \|D^l y - \sum_{i=1}^p \sum_n \sum_{k \in \Gamma_n} d_{i,k}^{(n)} D^l x_{i,k}^{(n)}\|_2^2 \geq \|y - \sum_{i=1}^p \sum_n \sum_{k \in \Gamma_n} d_{i,k}^{(n)} x_{i,k}^{(n)}\|_2^2 \quad (23)$$

Therefore, further modifications to the test function and its derivatives are required. The test function and the related derivatives are normalized as:

$$\bar{\omega}^l = \frac{\omega^{(l)}}{\|\omega^{(l)}\|_2}, l = 1, 2, \dots, m \quad (24)$$

which satisfies $\int_{[0, T]} \bar{\omega}^l(t) dt = 1$. The normalized test functions ensure that each data from the modulated function $y^l(\tau)$ has the same weight in the criterion as the signal in the raw datum $y(t)$ [33]. Now the representation of the ULS criterion given by (17) can be re-written as follows:

$$J_H = \left\| y - \sum_{i=1}^p \sum_n \sum_{k \in \Gamma_n} d_{i,k}^{(n)} \overline{x_{i,k}^{(n)}} \right\|_2^2 + \sum_{l=1}^m \left\| y^l - \sum_{i=1}^p \sum_n \sum_{k \in \Gamma_n} d_{i,k}^{(n)} \overline{(x_{i,k}^{(n)})^l} \right\|_2^2 \quad (25)$$

The discrete-time expression of the modulation procedure can be represented as:

$$\bar{y}^l(k) = \sum_{n=k}^{k+n_0} y(n) \bar{\omega}^l(n - k) \quad (26)$$

$$\overline{(x_{i,k}^{(n)})^l}(k) = \sum_{n=k}^{k+n_0} x_{i,k}^{(n)}(n) \bar{\omega}^l(n - k) \quad (27)$$

where n_0 is the support of the discrete test function and $k=1, 2, \dots, N-n_0$. The following equation represents the matrix form of the ULS problem:

$$Y_{ULS} = \Phi_{ULS} \theta \quad (28)$$

where

$$Y_{ULS} = [y(1), \dots, y(N), \bar{y}^1(1), \dots, \bar{y}^1(N - n_0), \dots, \bar{y}^m(1), \dots, \bar{y}^m(N - n_0)]^T \quad (29)$$

$$\theta = [d_{0,k}^{(n)}(1), \dots, d_{p,k}^{(n)}(N), (d_{0,k}^{(1)})^1, \dots, (d_{0,k}^{(n)})^m(N - n_0)]^T \quad (30)$$

$$\phi_{ULS} = \begin{bmatrix} x_{1,k}^{(n)}(1) & \dots & x_{p,k}^{(n)}(1) \\ \vdots & \dots & \vdots \\ x_{1,k}^{(n)}(N) & \dots & x_{p,k}^{(n)}(N) \\ \overline{x_{1,k}^{(n)}}^{-1}(1) & \dots & \overline{x_{p,k}^{(n)}}^{-1}(1) \\ \vdots & \dots & \vdots \\ \overline{x_{1,k}^{(n)}}^m(N - n_0) & \dots & \overline{x_{p,k}^{(n)}}^m(N - n_0) \end{bmatrix} \quad (31)$$

where Y_{ULS} is an output vector of size $[(m+1)N - mn_0] \times 1$, ϕ_{ULS} is the regression matrix of size $((m+1)N - mn_0) \times pM$ and θ is the time-invariant coefficient vector of size $pM \times 1$.

3.2 Model order determination

For many dynamic regression problems, the equation (28) may initially involve a large number of candidate model terms (i.e., regressors), an effective model reduction method is often highly needed for generating parsimonious models. The proposed UROFR algorithm is demonstrated to be robust for model term selection and parameter estimation. As for model order determination, one effective solution is to exploit several metrics that balance the trade-off between model complexity and model fit, including the famous Akaike information criterion (AIC) and Bayesian information criterion (BIC) which are as follows:

$$AIC(p) = \ln(\hat{\sigma}_p^2) + \frac{2p}{N} \quad (32)$$

$$BIC(p) = \ln(\hat{\sigma}_p^2) + \frac{p}{N} \ln(N) \quad (33)$$

where $\hat{\sigma}_p^2$ is the variance of the model residuals calculated from the associated model of order p , N is the sampled signals length. Both AIC and BIC include a penalty term associated to the number of model coefficients. The penalty of BIC is larger than that of AIC, which means that the best order determined according to the BIC criterion is often smaller than that given by AIC [34-36].

3.3 High-Resolution time-frequency Analysis based on Power Spectrum Density

The proposed TVAR-MWBF modeling approach can produce a high-resolution time-frequency representation for nonstationary signals. Once the initial full candidate time-varying model (1) refined and parameter estimates of the reduced model are obtained, the time-dependent power spectrum estimation then be accomplished as follows [5]:

$$PSD(t, f) = \frac{\hat{\sigma}_\varepsilon^2}{|1 - \sum_{i=1}^p \hat{a}_i(t) e^{-j2\pi i f / f_s}|^2} \quad (34)$$

where f and f_s are the natural (physical) frequency and sampling frequency, respectively. $\hat{a}_i(t)$ is the TVAR

parameters estimated at time t , $j = \sqrt{-1}$, and $\hat{\sigma}_\varepsilon^2$ is the variance of the estimated residual. The formula of the time-frequency function (34) is continuous concerning the frequency f . Thus it can be used for spectral estimation of any frequency point lower than the Nyquist frequency $f_s/2$. The frequency resolution is primarily not infinite and is related to the model order and the accuracy of parameter estimation.

The PSD distribution calculated by the spectral function (34) is utilized to extract time-frequency features of the nonstationary EEG signals. Considering the knowledge of clinical medical experience, the energy distribution characteristics of EEG signals are obtained by mesh band division in both the time and frequency domains [37]. Specially, three equal-sized windows and five sub-bands from the frequency domain are chosen in the present study. Fig. 2 shows a sample PSD distribution which is employed for feature extraction using a dashed grid.

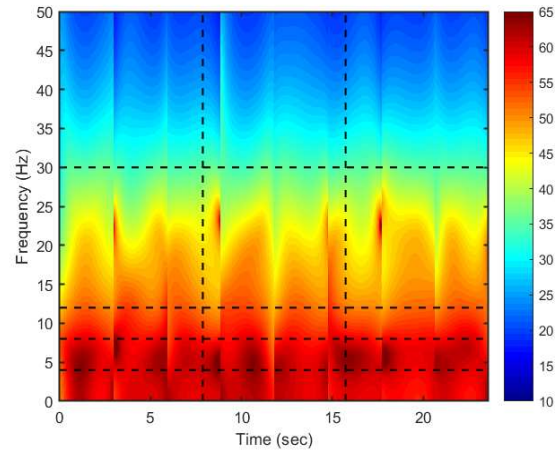


Fig. 2 A sample PSD distribution result with dotted grid by using three time windows and five frequency sub-bands for feature extraction

Each feature $F(a, b)$ is estimated as:

$$F(a, b) = \int_{t_a} \int_{f_b} PSD_y(t, f) df dt \quad (35)$$

where PSD_y is the PSD of the nonstationary time series y estimated using the aforementioned approach. The frequency sub-bands, which were defined according to the medical knowledge including delta(0-4HZ), theta(4-8HZ), alpha(8-12HZ), beta(12-30HZ) and gamma(30-50HZ), respectively. The size of the time window is determined by

the expertise of the neurologist consisting of $t_1(0\sim 7.87s)$, $t_2(7.87\sim 15.73s)$ and $t_3(15.73\sim 23.6s)$.

The integral formula (35) is equivalent to $F(a, b) = \sum_{t \in t_a} \sum_{f \in f_b} PSD_y(t, f)$ as PSD_y is discrete. Each feature represents the divisional energy of the time series over a particular frequency band and time window; consequently, the feature set describes the energy distribution of the

3.4 Classification and performance evaluation

The time-frequency energy distribution image is a high-dimensional vector that generally consists of redundant features. In such a situation, it is certainly desirable to remove these unnecessary features from the original TF representation through, for example the principal component analysis (PCA) algorithms and select an optimal feature subset for seizure detection. Once the optimal sub-feature set is chosen, the generated features are fed to an SVM classifier to implement the classification task. To select the best SVM parameters, a Bayesian optimization algorithm is adopted to improve the search efficiency. Meanwhile, the complete historical information is used to improve the computation speed. Following the conventional practice, the classification performance of the proposed approach can be assessed by several statistical metrics such as sensitivity (SEN), specificity (SPE), and accuracy (ACC). These measures of SEN, SPE, and ACC are summarized below:

$$SEN = \frac{TP}{TP+FN} \times 100\%$$

$$SPE = \frac{TN}{TN+FP} \times 100\%$$

$$ACC = \frac{TP+TN}{TP+TN+FP+FN} \times 100\%$$

where TP, TN, FP, and FN represent true positive (e.g., seizure identified as seizure), true negative (e.g., non-seizure identified as non-seizure), false positive (e.g., non-seizure identified as seizure) and false negative (e.g., seizure identified as non-seizure) separately.

To achieve an unbiased measure of the classification performance, 10-fold cross-validation was applied to verify the proposed method. After a round of ten-fold cross-validation, ten classification results are obtained. The average of the ten test results is calculated and used as the performance metric. In this paper, a total of ten rounds of ten-fold cross-validation are conducted, and the average of the ten rounds is reported as the final result. Therefore, the proposed method is unlikely to be influenced by way of how the data is sliced since each individual sample is used nine times in the training stage and once in the test stage.

4 Experimental results

signal in the time-frequency plane. It is required that the feature set should contain adequate information about the non-stationary characteristic of the signal. Thus, the total energy of the signal is involved as an additional feature. Thus, the feature vector of each data set is 16 dimensions ($3 \times 5 + 1$) [37].

In order to show the applicability and effectiveness of the proposed approach, both clean and noisy EEG data are considered for validation. We first examine this method in the two benchmark datasets mentioned in section 2, and then test the robustness of the proposed method for seizure detection against the EEG signals contaminated by muscle artifacts.

In the experiment, the TVAR-MWBF-UROFR method is adopted to model the real EEG data. The B-splines of order from 1 to 4 were utilized as the basis functions to construct TVAR models. Simulation results suggested that the order of the TVAR model (1) can be chosen to be 5. The estimates of the five time-varying parameters $a_i(t)$ ($i = 1, 2, 3, 4, 5$) are then attained by the UROFR method. In the UROFR algorithm, the cubic B-spline basis function was utilized as the modulating function and the first and second-order derivatives of the non-stationary signals are considered in the ULS criterion.

Fig. 3 shows a comparison between the recovered signal by the identified TVAR model and the original EEG time series. Note that only data points from 2s to 4s are presented in Fig. 3 for a clear visualization. It follows that the resulting TVAR model provides an extremely satisfactory representation of the EEG data, thus further time-frequency analysis can be carried out using the model.

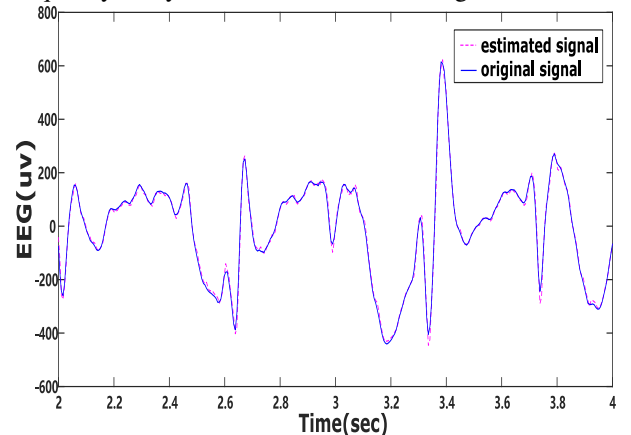


Fig. 3 A sample illustration of the recovered EEG signal and the original signal. The original signal was obtained from subset S of dataset 1.

As mentioned earlier, the power spectrum estimates calculated based on (34) is utilized to extract time-frequency features of the EEG data. The extracted features are then used for the binary classification tasks described in Section 2. Fig. 4a provides the accuracy performance acquired from five different classifiers. Obviously, the accuracy of

the SVM classifier is significantly better than other classifiers, and the finding here is in line with those reported in previous studies [15,38-40]. Although SVM outperformed Random Forest in this study, it is worth mentioning that researchers employed Systematic Forest and Forest CERN

to obtained 100% accuracy for seizure detection while reducing the detection time in literature [41]. Fig. 4b compares the accuracy obtained from two model structure selection algorithms (orthogonal forward regression and ultra-orthogonal forward regression) using the SVM classi-

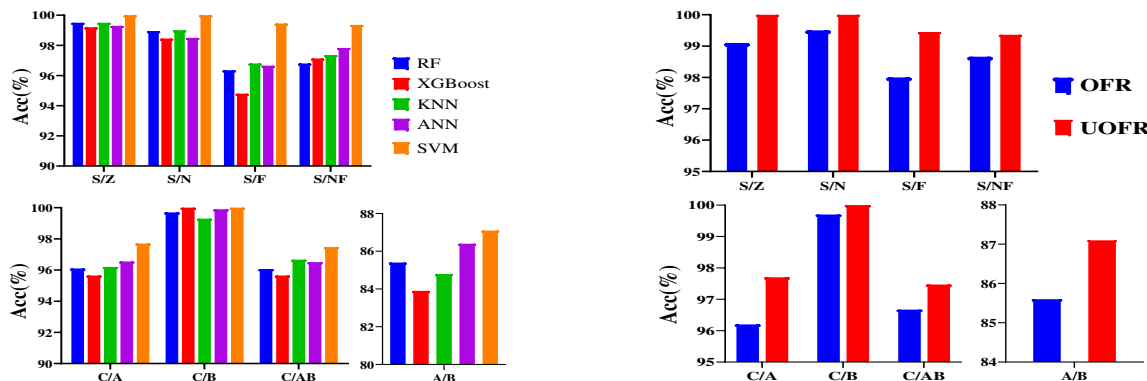


Fig. 4 (a) The accuracy of five classifiers (RF, XGBoost, KNN, ANN and SVM), and (b) The accuracy of the two algorithms (OFR and UOFR).

er, and what stands out in this figure is that the accuracy of the newly introduced UROFR algorithm is higher than that of the OFR algorithm in each classification task. These results indicate that the time-varying model identified by the proposed UROFR approach has better performance.

To further check the reliability and applicability of the features extracted from the TVAR model via the PSD estimation, we tested the influence of feature reduction and non-reduction on classification performance. Experimental results are listed in Table 1 and Table 2, where it can be noticed that satisfactory classification results were obtained without using PCA for feature dimension reduction (All the classification accuracy of seizure is above 95%, which can meet the requirements for various clinical conditions). These results provide further support for the effectiveness and robustness of our method. Moreover, it is evident from the tables that, the use of PCA based dimensionality reduction can further improve classification performance due to the removal of redundant correlated features. A notable finding is in the case of distinguishing pre-ictal and inter-ictal(A-B), the classification results presented relatively low accuracy (85.4% and 87.1%). This is understandable since the similarity between the two types of EEG signals was relatively high. In addition, compared with the method in literature [42], the accuracy of A-B is raised by 12.5% using our method (87.1% versus 74.6%).

Both dataset 1 and dataset 2 have been processed to remove artifacts before public release. However, in some clinical situations, it is impractical to exclude artifacts. Ref. [43] provides a review of the most common artifacts (e.g., muscle artifacts, eyes blinking, and ambient noise) presented in EEG signals. In this study, we modeled the

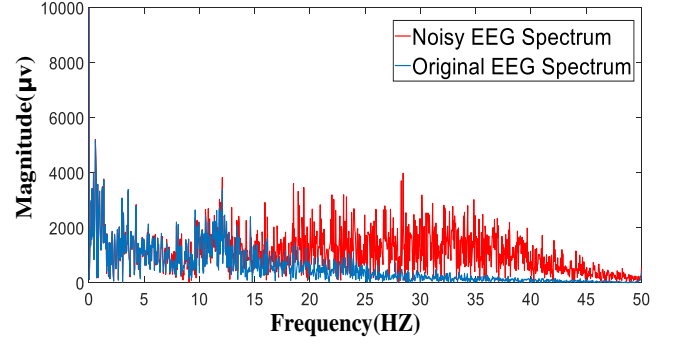
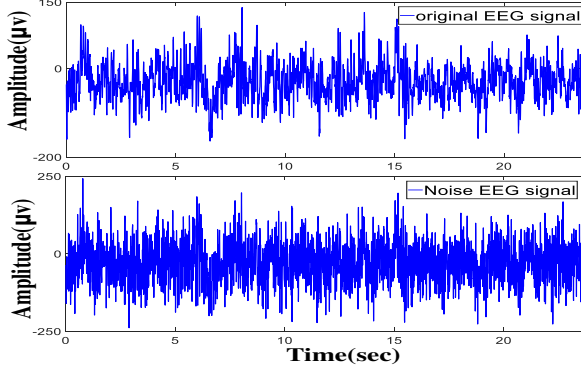
inevitable source of artifacts (i.e., muscle artifacts) using random noise filtered with a band-pass filter of 20Hz to 60 Hz and added them to original EEG data as described in [43,44]. The amplitude of muscle artifacts can be adapted to generate noisy EEG signals with different signal-to-noise-ratios (SNRs). Fig. 5a shows the changes in time-domain after adding simulated muscle artifacts, and Fig. 5b displays the difference in frequency spectrum. Note that the EEG signal was sampled from subset Z of dataset 1 and the SNR value is equal to 0 dB in this example. It is evident from those figures that the muscle artifacts appreciably change the characteristics of the original EEG signals, and thus may adversely affect the performance of seizure detection.

Table 1. feature dimension effect on classification (dataset 1)

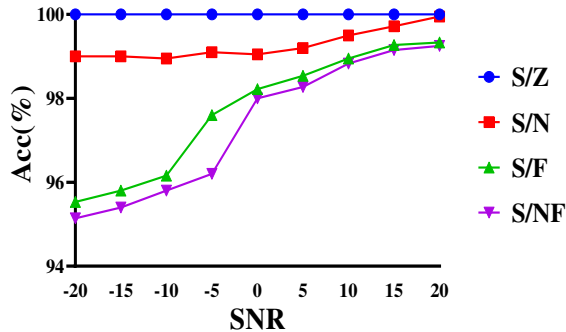
| Subsets | Metrics | Feature Set | |
|---------|---------|--------------|---------------------|
| | | No reduction | Reduced via PCA |
| S-F | SEN | 97.06 ± 0.80 | 100.0 ± 0.00 |
| | SPN | 97.43 ± 0.64 | 98.85 ± 0.41 |
| | ACC | 97.25 ± 0.59 | 99.45 ± 0.16 |
| S-Z | SEN | 100.0 ± 0.00 | 100.0 ± 0.00 |
| | SPN | 100.0 ± 0.00 | 100.0 ± 0.00 |
| | ACC | 100.0 ± 0.00 | 100.0 ± 0.00 |
| S-N | SEN | 99.28 ± 0.54 | 100.0 ± 0.00 |
| | SPN | 100.0 ± 0.00 | 100.0 ± 0.00 |
| | ACC | 99.65 ± 0.34 | 100.0 ± 0.00 |
| S-NF | SEN | 99.51 ± 0.25 | 99.89 ± 0.21 |
| | SPN | 97.53 ± 0.70 | 98.43 ± 0.68 |
| | ACC | 98.83 ± 0.18 | 99.36 ± 0.40 |

Table 2. feature dimension effect on classification (dataset 2)

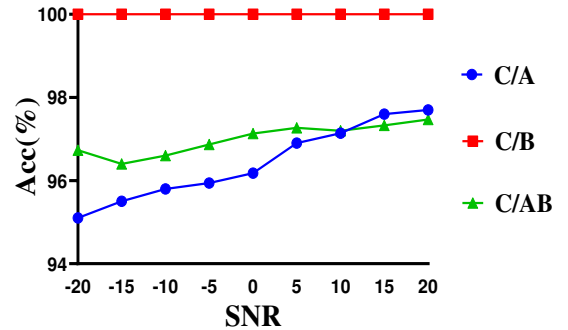
| Subsets | Metrics | Feature Set | |
|---------|---------|--------------|---------------------|
| | | No reduction | Reduced via PCA |
| C-A | SEN | 98.13 ± 0.43 | 99.42 ± 1.25 |
| | SPN | 95.34 ± 1.22 | 95.99 ± 0.99 |
| | ACC | 96.40 ± 0.84 | 97.70 ± 0.48 |
| C-B | SEN | 100.0 ± 0.00 | 100.0 ± 0.00 |
| | SPN | 100.0 ± 0.00 | 100.0 ± 0.00 |
| | ACC | 100.0 ± 0.00 | 100.0 ± 0.00 |

**Fig. 5** (a) An example of the noisy and the original signal, and (b) The example frequency spectrum of noisy and original EEG signals.

Therefore, this paper examines the practicability of our method in recognizing the seizure and non-seizure activities from EEG recordings with perceptible muscle artifacts. In the presence of muscle artifact within a certain range of SNR (-20 to 20dB), Fig. 6 presents the classification result obtained with the proposed technique using two datasets. There are several intriguing observations from this illustration worth highlighting. Firstly, the accuracy of seizure detection is maintained above 95% at all levels of noise, which is much better than the reported performance in the literature e.g. [45] where the accuracy dropped by approximately 10% in a medium-level noise (i.e., SNR=5dB).



This result clearly indicates the strong robustness of our method in detecting epileptic seizures when the EEG signals were obscured by muscle artifacts. Another interesting finding is that, for classification tasks S/Z (i.e., epileptic seizure versus healthy brain activities), and C/B (i.e., ictal versus inter-ictal), even if the EEG signals were entirely buried in artifacts (i.e., SNR=-20dB), our proposed method still worked with 100% accuracy. This performance is better than that reported in [44], and provides further evidence that this method has the ability to recognize seizure EEG from non-resting EEG with muscle artifacts.

**Fig. 6** The change trend of seizure detection result obtained with the proposed method using two datasets in the presence of muscle artifacts

MWBF-UOFR). Fig. 7 and Fig. 8 present the TF images of EEG segments from dataset 1 and dataset 2, respectively. The most prominent finding from these illustrations is that the PSD distribution of the epileptic seizure EEG data (i.e., Set S and Set C) are significantly higher than that of other types of data. This is concordant with our previous

the change trend of seizure detection result obtained with the proposed method using two datasets in the presence of muscle artifacts (MWBF-UOFR). Fig. 7 and Fig. 8 present the TF images of EEG segments from dataset 1 and dataset 2, respectively. The most prominent finding from these illustrations is that the PSD distribution of the epileptic seizure EEG data (i.e., Set S and Set C) are significantly higher than that of other types of data. This is concordant with our previous

observations [5,22,37]. Among the four time-frequency analysis methods, the STFT method cannot acquire high temporal resolution and frequency resolution at the same time; in fact, its resolution is fixed and cannot be changed once the window function is selected. Although the CWT approach achieves a good trade-off between the temporal and frequency resolutions by using a narrow window in high frequency and a wide window in low frequency, it is difficult to accurately realize a high resolution in both low and high-frequency areas at the same time; this may degrade temporal resolution for low-frequency components and frequency resolution for high-frequency components. Compared with the STFT and CWT methods, the multi-wavelet basis function expansion method, however, can

capture quite a useful transient information of the inherent nonstationary dynamics in correlated EEG movements, thereby obtaining higher time-frequency resolution. A closer inspection of these plots shows that the time-frequency images generated by the UROFR algorithm are much sharper and better defined, and precisely reflect the

distribution of local frequency components changes across time. These results further confirm the superiority of the proposed TVAR-MWBF-UROFR method to other compared methods, proving its improved performance for modeling and feature extraction of the EEG time series.

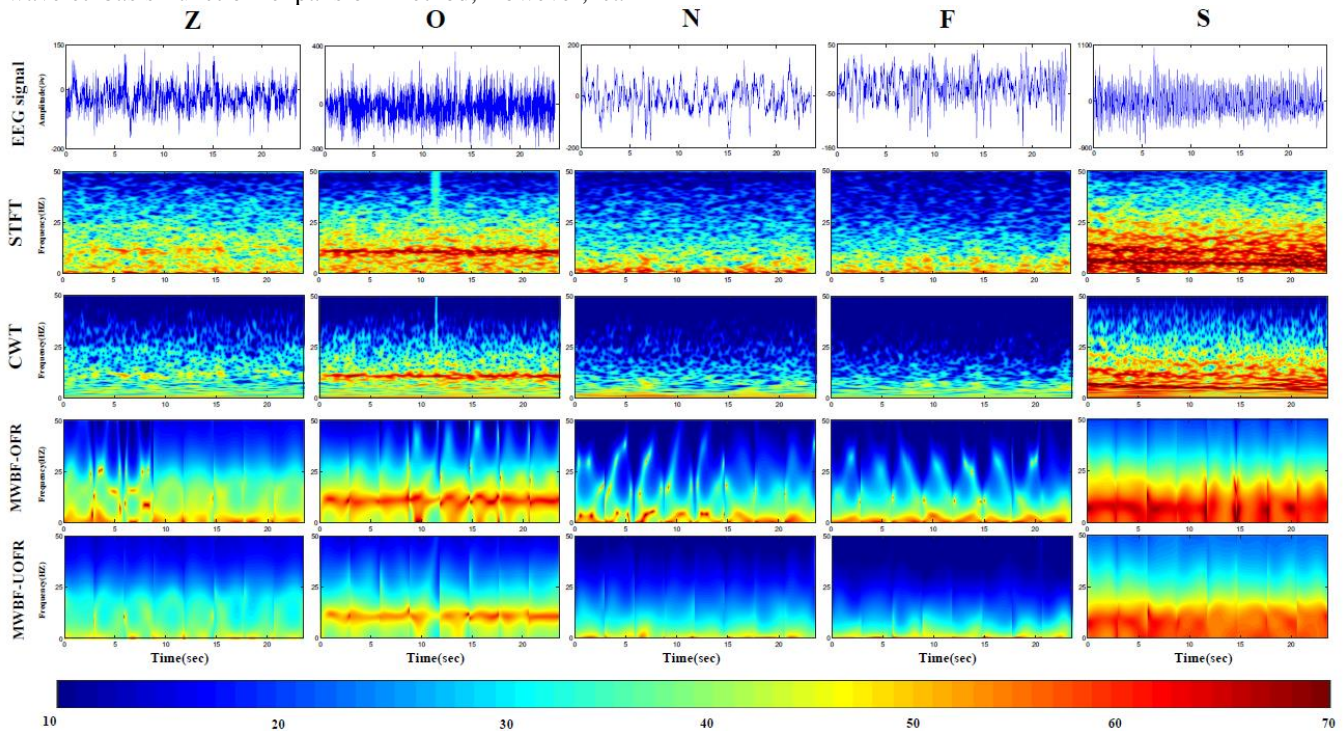


Fig. 7 The PSD energy features of EEG segments by different time-frequency methods (obtained from dataset 1).

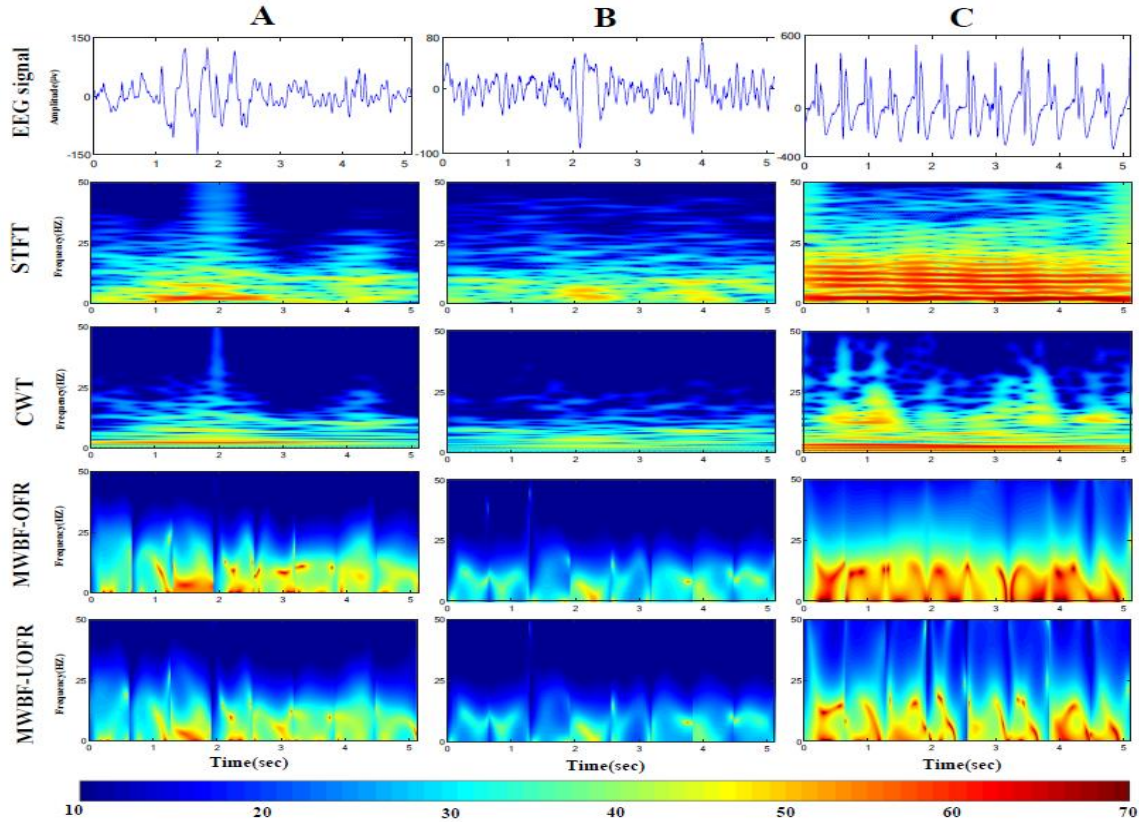


Fig.8 The PSD energy features of EEG segments by different time-frequency methods (obtained from dataset 2).

5 Discussion

Linear techniques have been extensively used in the field of time-frequency analysis, primarily because of their straightforward and adaptability. However, linear modeling methods may not be adequate to represent a nonlinear system and may result in the loss of some potentially related and important information [46]. To overcome the limitations of linear models, time-varying nonlinear models can be adopted to achieve more reliable analysis results.

The implementation and identification of time-varying nonlinear models, however, may be very complicated. Thus, this study proposes a new multi-resolution wavelet expansion and UOFR method for TVAR model identification and time-frequency analysis. Building a TVAR model instead of a traditional time-invariant AR model makes the model more flexible and suitable for capturing transient changes in non-stationary signals such as EEG data.

Table 3. Performance comparison of different methods for seizure classification

| Authors and year | Methods | Task | Accuracy(%) |
|----------------------------|---|----------|--------------|
| Polat et al.[47] (2007) | FFT-decision tree classifier | | 98.72 |
| Wang et al.[48] (2011) | Wavelet transform and Shanon entropy k-nearest neighbor | | 99-100 |
| Fu et al.[49] (2015) | Hilbert-Huang transform, Support vector machine | S and Z | 99.125 |
| Houssein et al.[50] (2018) | Grasshopper Optimization Algorithm (GOA) and SVM | | 100 |
| This work | TVAR-MWBF-UOFR, SVM, Bayesian optimization | | 100 |
| Tawfik et al.[51] (2016) | Weighted Per-mutation Entropy (WPE) and SVM | | 96.50 |
| Hassan et al.[52] (2016) | CEEMDAN and linear programming boosting classifier | S and F | 97.40 |
| Li et al.[53] (2019) | MRBF-MPSO-OLS, GLCM+FV, and SVM | | 99.30 |
| This work | TVAR-MWBF-UOFR, SVM, Bayesian optimization | | 99.45 |
| Zhu et al.[54] (2014) | Degree and strength of HVG and K-nearest neighbor (K-NN) classifier | | 98 |
| Sharma et al.[55] (2017) | ATFFWT and FD feature using LS-SVM | S and N | 99 |
| Siddiqui et al.[41] (2019) | Brain data mining, Systematic Forest (SysFor) and Forest CERN | | 100 |
| This work | TVAR-MWBF-UOFR, SVM, Bayesian optimization | | 100 |
| Joshi et al.[56] (2014) | FLP error energy and signal energy and SVM classifier | S and NF | 95.33 |

| | | |
|----------------------------------|--|--------------|
| Rajeev Sharma et al. [57] (2015) | 95% Confidence area measure of 2D PSR of IMFs, IQR of Euclidian distance of 3D PSR of IMFs and LS-SVM classifier | 98.67 |
| Li et al. [5] (2018) | MRBF-MPSO, PSD, PCA, Support vector machines | 98.73 |
| Matin et al. [58] (2019) | A hybrid dimension reduction model utilizing Independent and Principal Component Analysis (ICA, PCA) and SVM | 98.93 |
| This work | TVAR-MWBF-UROFR, SVM, Bayesian optimization | 99.36 |

Bold values indicate better results of the proposed method than other method

To make a comprehensive performance comparison, we compare the proposed method with the other existing well-known algorithms. Table 3 presents the classification accuracy of a number of state-of-the-art methods applied to the benchmark Bonn dada (Dataset 1). As can be seen from Table 3, the TVAR-MWBF-UROFR approach shows the best performance for all classification tasks. Specifically, in discrimination tasks, both S/Z and S/N reach 100% accuracy, and the accuracy of task S/F, S/NF achieve state-of-the-art results. On the dataset 2, Gupta et al. [42] and Li et al. [53] attained average classification accuracy of 79.70%, 96.50%, 91.80%, 74.60% and 97.40%, 99.30%, 98.20%, 85.70% for cases of C-A, C-B, C-AB and A-B, respectively. For the purpose of comparison, our method yielded better results with an accuracy of 97.70%, 100%, 97.47%, and 87.10%. The achievement of high classification accuracy of the proposed approach is primarily attributed to the following factors: a) the use of multi-wavelets as building blocks for TVAR model construction; b) an effective ultra-regularized UROFR is utilized for model reduction; c) a time-frequency power spectrum density (PSD) estimation approach is employed for feature extraction; d) SVM hyperparameters determining was performed with Bayesian optimization. These factors combined enable the proposed TVAR-MWBF-UROFR framework to become a powerful and valuable tool for EEG signal modelling and epileptic seizure detection.

Although the proposed method shows excellent performances when applied to the two benchmark datasets, as demonstrated through a series of comprehensive validation studies in Section 4, it still has two limitations. The first disadvantage is the computational cost of the ULS criterion was large. To make use of the derivative information, several simultaneous equation regression models are involved, as defined in Eq. 31. However, compared with a steady improvement in identification performance, this computational problem may become less important after exploiting a high-performance computing machine. Another potential drawback is that we did not get further insight into the effect of different frequency bands' activities (i.e., delta, theta, alpha, beta, and gamma) on the initiation of epileptic seizures. In this work, PCA was adopted to select an optimal subset from the original time-frequency representation for classification and obtain a better result; this is because the PCA techniques can eliminate the mutual influence factors of the raw components, and thus attain the

most discriminative features. But this did not locate to the specific frequency components that are associated with seizures. Therefore, we will extend our study to better understand the mechanisms underlying epilepsy seizure in the future with the help of the clinicians.

6 Conclusion

This paper presents an effective TVAR-MWBF-UROFR scheme for the time-frequency analysis of non-stationary dynamic processes such as EEG signals. The proposed framework mainly includes three key points. Firstly, a useful modeling approach based on multi-wavelet basis function expansion is introduced. The UROFR algorithm is then employed to determine a parsimonious model with satisfying generalization performance. Secondly, the time-varying PSD function is defined (Eq. 34) and utilized to calculate power distributions of the EEG signals. Thirdly, the resulting feature vectors are processed using PCA and fed to different classifiers. A Bayesian optimization approach is applied to these classifiers to adjust the relevant parameters automatically.

The promising results reported in Section 4 confirm that the proposed TVAR-MWBF-UROFR approach performs well for seizure detection from EEG data (including clean EEG data and noisy EEG data). Therefore, the method is potentially applicable to clinical practice for seizure detection. The achievement of the good performance of the novel approach is attributed to the employment of multi-wavelet expansions and the UOFR algorithm, which can produce a parsimonious TVAR model for a simplified description of dynamical systems. Thus it is able to reveal the precise mapping of time-frequency components and capture the transient characteristics of non-stationary processes. Additionally, the obtained high-resolution TF images based on PSD provide useful information about the temporal evolution of transient frequency components; this contributes to helping clinicians understand the pathogenesis of epilepsy through seizure EEG TF images. Therefore, this work offers valuable insights into developing an interpretive automatic epileptic detection system (e.g., a detector). Further research would be undertaken to explore how to build an end-to-end real-time online seizure monitor with explicit medical and physical meanings based on the

proposed approach. Relevant results will be presented in future separate publications.

Appendix

Derivation of the ROFR algorithm.

Consider the matrix form of model (6):

$$y = \Psi_M c + e$$

$$\begin{cases} y = [y(1), y(2), \dots, y(N)]^T \\ \Psi_M = [\psi(1), \psi(2), \dots, \psi(N)]^T \\ e = [e(1), e(2), \dots, e(N)]^T \end{cases} \quad (36)$$

Define the orthogonal decomposition of the regression matrix as:

$$\Psi_M = [w_1, w_2, \dots, w_n] \begin{bmatrix} 1 & \alpha_{1,2} & \dots & \alpha_{1,N} \\ 0 & 1 & \dots & \vdots \\ \vdots & \vdots & \ddots & \alpha_{N-1,N} \\ 0 & \dots & 0 & 1 \end{bmatrix} = WA \quad (37)$$

where the orthogonal columns satisfying $w_i^T w_j = 0, i \neq j$.

The model can be rewritten as:

$$Y = Wg + e \quad (38)$$

where the orthogonal weight vector $g = [g_1, g_2, \dots, g_N]^T$ and the parameter vector c satisfying $Ac = g$.

The ROLS algorithm considers the zero-order regularization error, and its standardized error criterion is:

$$\frac{(e^T e + \lambda g^T g)}{y^T y} = 1 - \sum_{i=1}^N \frac{[(w_i^T w + \lambda) g_i^2]}{y^T y} = 1 - \sum_{i=1}^N \Delta e_i \quad (39)$$

where $\lambda \geq 0$ is the regularization parameter, Δe_i is the regularized error reduction ratio. An elegant method to determine the regularization parameter is to employ a Bayesian interpretation to the ROLS algorithm which results in the following iterative procedure for calculating λ :

$$\lambda = \frac{\eta}{N - \eta} \cdot \frac{e^T e}{g^T g} \quad (40)$$

$$\eta = \sum_i \frac{w_i^T w_i}{w_i^T w_i + \lambda} \quad (41)$$

Given an initial value λ_0 , after a few iterative calculations, a stable and algorithmic value can be obtained. Actually, λ was elected to be one in this paper. The pseudo code of the UROFR algorithm is shown below.

Pseudo code for the ROFR algorithm (refer to Eq.(28))

Input:

Output signal: $Y = Y_{ULS}$
Candidate terms: $\phi_{ULS} = \phi_i, i = 1, 2, \dots, pM$
Regularization parameter: $\lambda \geq 0$
Predetermined threshold: τ

Step 1. Set $I_1 = \{1, 2, \dots, pM\}, S = pM, \sigma = Y^T Y$;
for $i = 1$ to S :

$$w_i = \phi_i;$$

$$RERR_i = \frac{\langle Y, w_i \rangle^2}{\sigma \langle (w_i, w) + \lambda \rangle} \times 100\%; \quad a_{11} = 1$$

end for

$$h_1 = \operatorname{argmax}_{i \in I_1} \{RERR_i\}; \quad w_1^0 = w_h$$

$$g_1^0 = \frac{\langle Y, w_1^0 \rangle}{\langle (w_1^0, w_1^0) + \lambda \rangle};$$

Setp j. $j \geq 2$:

for $j = 2$ to S :

$$I_j = I_{j-1} \setminus \{h_{j-1}\};$$

for all $i \in I_j$:

$$w_i = \phi_i - \sum_{k=1}^{j-1} \frac{\langle \phi_i, w_k^0 \rangle}{\langle w_k^0, w_k^0 \rangle} w_k^0$$

$$RERR_i = \frac{\langle Y, w_i \rangle^2}{\sigma \langle (w_i, w) + \lambda \rangle} \times 100\%$$

end for (end loop i)

$$J_j = \{ \operatorname{arg} g_{i \in I_j} (w_i^T w_i < \tau) \}; \quad I_j = I_j \setminus J_j;$$

$$h_j = \operatorname{argmax}_{i \in I_j} \{RERR_i\}; \quad w_j^0 = w_{h_j};$$

$$g_j^0 = \frac{\langle Y, w_j^0 \rangle}{\langle (w_j^0, w_j^0) + \lambda \rangle}; \quad a_{jj} = 1$$

for $k=1$ to $j-1$:

$$a_{kj} = \frac{\langle w_k^0, \phi_{h_j} \rangle}{\langle w_k^0, w_k^0 \rangle};$$

end for (end loop for k)

end for (end loop for j)

Output:

Selected model term: $\phi = [\phi_1, \phi_2, \dots, \phi_l]$

Term parameter: θ

Acknowledgments: This work was supported in part by the Engineering and Physical Sciences Research Council (EPSRC) under Grant EP/I011056/1; EPSRC Platform Grant EP/H00453X/1; the Royal Society – International Exchanges (IES\R3\183107 - Neurophysiological Biomarkers for Comparative Diagnosis and Prognosis across Neurodegenerative Diseases); Alzheimer Research UK (Developing a new biomarker for the early diagnosis of dementia; a novel non-linear signal processing approach using resting state EEG); Ryder Briggs Charity (The thalamic clock and the cortical focus theory in childhood absence epilepsy an insight with a new approach of quantitative EEG analysis in the time domain: the error reduction ratio method).

Compliance with ethical standards

Conflicts of Interest: The authors declare no conflict of interest.

References

- Acharya UR, Subbhuraam VS, Ang P, Yanti R, Suri J (2012) Application of non-linear and wavelet based features for the automated identification of epileptic EEG signals. International journal of neural systems 22:1250002.
- Mormann F, Andrzejak R, Elger C, Lehnertz K (2007) Seizure prediction: The long and winding road. Brain : a journal of neurology 130:314-333. doi:10.1093/brain/awl241
- Tzallas A, Tsipouras M, Fotiadis D (2007) Automatic Seizure Detection Based on Time-Frequency Analysis and Artificial Neural Networks. Computational intelligence and neuroscience 2007:80510. doi:10.1155/2007/80510
- Wang L, Xue W, Li Y, Luo M, Huang J, Cui W, Huang C (2017) Automatic Epileptic Seizure Detection in EEG Signals Using Multi-Domain Feature Extraction and Nonlinear Analysis. Entropy 19:222.

5. Li Y, Wang X, Luo M, Li K, Yang X, Guo Q (2018) Epileptic Seizure Classification of EEGs Using Time-Frequency Analysis Based Multiscale Radial Basis Functions. *IEEE Journal of Biomedical and Health Informatics* 22 (2):386-397.
6. Giannakakis G, Sakkalis V, PEDIADITIS M, Tsiknakis M (2014) Methods for seizure detection and prediction: an overview. In: *Modern Electroencephalographic Assessment Techniques*. Springer, pp 131-157
7. Zhang Z, Hung Y, Chan S (2011) Local Polynomial Modeling of Time-Varying Autoregressive Models With Application to Time-Frequency Analysis of Event-Related EEG. *IEEE transactions on biomedical engineering* 58:557-566.
8. Hassan AR, Siuly S, Zhang Y (2016) Epileptic seizure detection in EEG signals using tunable-Q factor wavelet transform and bootstrap aggregating. *Computer methods and programs in biomedicine* 137:247-259
9. Sengur A, Guo Y, Akbulut Y (2016) Time-frequency texture descriptors of EEG signals for efficient detection of epileptic seizure. *Brain Informatics* 3:1-8. doi:10.1007/s40708-015-0029-8
10. Wilson S, Emerson R (2003) Spike detection: a review and comparison of algorithms. *Clinical neurophysiology : official journal of the International Federation of Clinical Neurophysiology* 113:1873-1881. doi:10.1016/S1388-2457(02)00297-3
11. Bajaj V, Pachori R (2012) Classification of seizure and nonseizure EEG signals using empirical mode decomposition. *IEEE Transactions on Information Technology in Biomedicine* 16:1135-1142. doi:10.1109/TITB.2011.2181403
12. Wang S, Wei H-L, Coca D, Billings S (2011) Model term selection for spatio-temporal system identification using mutual information. *International Journal of Systems Science - IJSySc* 44:1-9. doi:10.1080/00207721.2011.600468
13. Gandhi T, Panigrahi B, Anand S (2011) A comparative study of wavelet families for EEG signal classification. *Neurocomputing* 74:3051-3057. doi:10.1016/j.neucom.2011.04.029
14. Guo L, Rivero D, Pazos A (2010) Epileptic seizure detection using multiwavelet transform based approximate entropy and artificial neural networks. *Journal of neuroscience methods* 193:156-163. doi:10.1016/j.jneumeth.2010.08.030
15. Shufang L, Weidong Z, Qi Y, Shujuan G, Dongmei C (2013) Feature extraction and recognition of ictal EEG using EMD and SVM. *Computers in Biology & Medicine* 43 (7):807-816
16. Faust O, Acharya UR, Adeli H, Adeli A (2015) Wavelet-based EEG processing for computer-aided seizure detection and epilepsy diagnosis. *Seizure* 26:56-64
17. Wani S, Sabut S, Nalbalwar S (2019) Detection of Epileptic Seizure Using Wavelet Transform and Neural Network Classifier. In: *Computing, Communication and Signal Processing*. Springer, pp 739-747
18. Li Y, Cui W-G, Luo M-L, Li K, Wang L (2017) High-resolution time-frequency representation of EEG data using multi-scale wavelets. *International Journal of Systems Science* 48:1-11.
19. Tuncer T, Dogan S, Akbal E (2019) A novel local senary pattern based epilepsy diagnosis system using EEG signals. *Australasian Physical & Engineering Sciences in Medicine*. doi:10.1007/s13246-019-00794-x
20. Wei H-L, Billings S (2002) Identification of time-varying systems using multiresolution wavelet models. *International Journal of Systems Science* 33 (15):1217-1228
21. Li Y, Luo M-L, Li K (2016) A multiwavelet-based time-varying model identification approach for time-frequency analysis of EEG signals. *Neurocomputing*. doi:10.1016/j.neucom.2016.01.062
22. Wei HL, Billings SA, Liu JJ (2010) Time-varying parametric modelling and time-dependent spectral characterisation with applications to EEG signals using multiwavelets. *International Journal of Modelling, Identification and Control* 9 (3):215-224
23. Li Y, Wei H, Billings SA (2011) Identification of Time-Varying Systems Using Multi-Wavelet Basis Functions. *IEEE Transactions on Control Systems Technology* 19 (3):656-663.
24. Song X, Li Y, Guo Q, Yang X-F, Chan R (2017) Identification of time-varying neural dynamics from spike train data using multiwavelet basis functions. *Journal of Neuroscience Methods* 278:46-56. doi:10.1016/j.jneumeth.2016.12.018
25. Andrzejak R, Lehnertz K, Mormann F, Rieke C, David P, Elger C (2002) Indications of nonlinear deterministic and finite-dimensional structures in time series of brain electrical activity: Dependence on recording region and brain state. *Physical review E, Statistical, nonlinear, and soft matter physics* 64:061907.
26. Billings SA, Jamaluddin HB, Chen S (1992) Properties of neural networks with applications to modelling non-linear dynamical systems. *International Journal of Control* 55 (1):193-224.
27. Mallat, S. G. (1989). A theory for multiresolution signal decomposition: the wavelet representation. *IEEE transactions on pattern analysis and machine intelligence*, 11(7), 674-693.
28. Graps A (1995) An introduction to wavelets. *IEEE computational science and engineering* 2 (2):50-61
29. Wei H-L, Billings SA, Balikhin M (2004) Prediction of the DST Index Using Multi-resolution Wavelet Models. *J Geophys Res* 109. doi:10.1029/2003JA010332
30. Wei H-L, Billings SA (2006) An efficient nonlinear cardinal B-spline model for high tide forecasts at the Venice Lagoon. *Nonlinear Processes in Geophysics* 13.
31. Wei H-L, Billings SA, Liu J (2004) Term and variable selection for non-linear system identification. *International Journal of Control* 77 (1):86-110
32. Guo Y, Guo L, Billings SA, Wei H-L (2015) An iterative orthogonal forward regression algorithm. *International Journal of Systems Science* 46 (5):776-789
33. Guo Y, Guo L, Billings S, Wei H-L (2016) Ultra-orthogonal forward regression algorithms for the identification of non-linear dynamic systems. *Neurocomputing* 173:715-723
34. Akaike H (1974) A New Look at the Statistical Model Identification. *Automatic Control IEEE Transactions on* 19 (6):716-723
35. Schwarz G (1978) Estimating the dimension of a model. *The annals of statistics* 6 (2):461-464
36. Efron B, Tibshirani RJ (2010) *An Introduction to the Bootstrap*. Teaching Statistics 23 (2):49-54
37. Tzallas A, Tsipouras M, Fotiadis D (2009) Epileptic Seizure Detection in EEGs Using Time-Frequency Analysis. *IEEE transactions on information technology in biomedicine*, 13(5), 703-710.
38. Yuan Q, Zhou W, Xu F, Leng Y, Wei D (2018) Epileptic EEG identification via LBP operators on wavelet coefficients. *International journal of neural systems* 28 (08):1850010
39. Zeng W, Li M, Yuan C, Wang Q, Liu F, Wang Y (2019) Identification of epileptic seizures in EEG signals using time-scale decomposition (ITD), discrete wavelet transform (DWT), phase space reconstruction (PSR) and neural networks. *Artificial Intelligence Review*. doi:10.1007/s10462-019-09755-y
40. Luigi C, Antonio M, Guido P, Marco S, Carmelo A, Gabriella C, Filomena F (2010) Real-time epileptic seizure prediction using AR models and support vector machines. *IEEE Transactions on Biomedical Engineering* 57 (5):1124-1132
41. Siddiqui MK, Islam MZ, Kabir MA (2019) A novel quick seizure detection and localization through brain data mining on ecog dataset. *Neural Computing and Applications* 31 (9):5595-5608
42. Gupta A, Singh P, Karlekar M (2018) A novel signal modeling approach for classification of seizure and seizure-free EEG signals. *IEEE Transactions on Neural Systems and Rehabilitation Engineering* 26 (5):925-935
43. Delorme A, Sejnowski T, Makeig S (2007) Enhanced detection of artifacts in EEG data using higher-order statistics and independent component analysis. *Neuroimage* 34 (4):1443-1449
44. Hussein R, Elgendi M, Wang ZJ, Ward RK (2018) Robust detection of epileptic seizures based on L1-penalized robust regression of EEG signals. *Expert Systems with Applications* 104:153-167
45. Abualsaud K, Mahmuddin M, Saleh M, Mohamed A (2015) Ensemble classifier for epileptic seizure detection for imperfect EEG data. *The Scientific World Journal* 2015
46. Guo Y, Wang L, Li Y, Luo J, Wang K, Billings SA, Guo L (2019)

Neural Activity Inspired Asymmetric Basis Function TV-NARX Model for the Identification of Time-Varying Dynamic Systems. *Neurocomputing* 357:188-202.

47. Polat K, Güneş S (2007) Classification of epileptiform EEG using a hybrid system based on decision tree classifier and fast Fourier transform. *Applied Mathematics and Computation* 187:1017-1026. doi:10.1016/j.amc.2006.09.022

48. Wang D, Miao D, Xmm C (2011) Best basis-based wavelet packet entropy feature extraction and hierarchical EEG classification for epileptic detection. *Expert Syst Appl* 38:14314-14320. doi:10.1016/j.eswa.2011.05.096

49. Fu K, Qu J, Chai Y, Zou T (2015) Hilbert marginal spectrum analysis for automatic seizure detection in EEG signals. *Biomedical Signal Processing and Control* 18:179-185

50. Hamad A, Houssein EH, Hassanien AE, Fahmy, A . A(2018) Hybrid grasshopper optimization algorithm and support vector machines for automatic seizure detection in EEG signals. In: *International Conference on Advanced Machine Learning Technologies and Applications*, 2018. Springer, pp 82-91

51. Tawfik NS, Youssef SM, Kholief M (2016) A hybrid automated detection of epileptic seizures in EEG records. *Computers & Electrical Engineering* 53:177-190

52. Hassan AR, Subasi A (2016) Automatic identification of epileptic seizures from EEG signals using linear programming boosting. *computer methods and programs in biomedicine* 136:65-77

53. Li Y, Cui W-G, Huang H, Guo Y-Z, Li K, Tan T (2019) Epileptic seizure detection in EEG signals using sparse multiscale radial basis function networks and the Fisher vector approach. *Knowledge-Based Systems* 164:96-106

54. Zhu G, Li Y, Wen PP (2014) Epileptic seizure detection in EEGs signals using a fast weighted horizontal visibility algorithm. *Computer methods and programs in biomedicine* 115 (2):64-75

55. Sharma M, Pachori RB, Acharya UR (2017) A new approach to characterize epileptic seizures using analytic time-frequency flexible wavelet transform and fractal dimension. *Pattern Recognition Letters* 94:172-179

56. Joshi V, Pachori R, Vijesh A (2014) Classification of ictal and seizure-free EEG signals using fractional linear prediction. *Biomedical Signal Processing and Control* 09:1-5.

57. Sharma R, Pachori RB (2015) Classification of epileptic seizures in EEG signals based on phase space representation of intrinsic mode functions. *Expert Systems with Applications* 42 (3):1106-1117

58. Matin A, Bhuiyan R A, Shafi S R, et al. A Hybrid Scheme Using PCA and ICA Based Statistical Feature for Epileptic Seizure Recognition from EEG Signal[C]//2019 Joint 8th International Conference on Informatics, Electronics & Vision (ICIEV) and 2019 3rd International Conference on Imaging, Vision & Pattern Recognition (icIVPR). IEEE, 2019: 301-306